Theoretical and experimental studies of metal-infiltrated opals

A. L. Pokrovsky, V. Kamaev, C. Y. Li, Z. V. Vardeny, and A. L. Efros*
University of Utah, Salt Lake City, Utah 84112, USA

D. A. Kurdyukov and V. G. Golubev
Ioffe Physico-Technical Institute, St. Petersburg, Russia

(Received 22 October 2004; revised manuscript received 28 January 2005; published 25 April 2005)

The optical properties of metal-infiltrated synthetic opals have been studied analytically, numerically, and experimentally in the visible and infrared spectral ranges. A simple model of weakly interacting resonant cavities is proposed to qualitatively understand the dispersion of electromagnetic waves in metallic photonic crystals. In the approximation of an ideal metal infiltrated into opals this model is exact, and the frequencies of the propagating modes in metallic opals are close to the eigenfrequencies of a single spherical resonator. Photonic band structures based on the dispersion of a metal dielectric constant have been calculated numerically for several metals and show similarity with the ideal metal model. Reflectivity and transmission spectra of thin-film metallic opals are calculated. Growth and saturation of the reflectivity spectra at low frequencies are manifestations of the omnidirectional band gap. The sharpest minimum in the reflectivity and maximum in the transmission spectra correspond to the position of the cutoff frequency. Silver- and copper-infiltrated opals were fabricated and their reflectivity spectra were measured in the visible to mid-IR spectral range. These spectra are in a good agreement with the theoretical calculations.

DOI: 10.1103/PhysRevB.71.165114 PACS number(s): 42.70.Qs, 42.25.Gy

I. INTRODUCTION

The idea underlying our studies of metallic photonic crystals is to create a medium with metallic dc conductivity and, at the same time, with transparency to electromagnetic (EM) waves in a desired frequency range. In this work we report on theoretical, numerical, and experimental studies of the optical properties of opal photonic crystals infiltrated with various metals.

Photonic spectra of a conducting metallic photonic crystal (MPC) differs from a dielectric photonic crystal in a low-frequency range. A dielectric crystal has a mode with a wavelength larger than the period of the crystal d. The spectrum of this mode is similar to a regular light, $\omega = ck/\sqrt{\epsilon_{av}}$, where ϵ_{av} is the average dielectric constant. This mode goes down to zero frequency.

Photonic spectra of the MPCs have an important and interesting feature, namely, a cutoff frequency ω_c. For $\omega < \omega_c$ there are no propagating EM modes.[1,2] The explanation for this phenomenon is as follows. When the EM wavelength is much larger than the period, d of the MPC, then the macroscopic dielectric constant $\epsilon(\omega)$ is an averaged dielectric constant of the metallic and dielectric constituents of the MPC. Therefore $\epsilon(\omega)$ has the form

$$\epsilon(\omega) = (1-f)\epsilon_d + fi\sigma/\omega, \tag{1}$$

where ϵ_d refers to the dielectric, σ is the metal's conductivity, and f is the volume-filling fraction of the metal. At small ω, ϵ is imaginary and $R=1$, which means that no EM waves can propagate in the MPC at such frequencies.

In this model we represent the MPC as a homogenious metal with the density of electrons fn, where n is the density in the metal. It is obvious that the cutoff frequency in this model is $\omega_c = \sqrt{f}\omega_p$, where ω_p is the plasma frequency of a metal.

However, taking into account a real structure of MPC, one can find the whole spectrum of the EM modes below this frequency. Their fields have a form of the Bloch functions and their propagation becomes possible because the distribution of electric field in the elementary cell is such that the field is small at the surfaces of the metallic constituents. However such a modulation increases the EM frequency so that the spectrum still has a cutoff frequency of the order of $\omega_c \approx 2\pi c/\sqrt{\epsilon_d} d$.[1,2]

Consequently, ω_c is determined by the lattice constant of the crystal and for MPCs with period of the order of millimeters, ω_c is in the gigahertz range. To fabricate a MPC capable of operating in the visible spectral range, one should have a lattice constant of $\sim 0.25\ \mu$m.[3–7]

One of the most promising three-dimensional metallic photonic crystal structures with such a small period are metal-infiltrated opals (MIOs).[3] Opal is a close-packed fcc photonic crystal formed by silica balls with a diameter D between 250 and 1500 nm.[8–10] The volume fraction of the empty pores in a bare, uninfiltrated opal is $\approx 26\%$. The structure of a bare opal photonic crystal and the dispersion of EM waves are shown in Fig. 1. One can see a low-energy mode typical for a dielectric photonic crystal.

The first computational study of opal replica (where the silica balls were substituted by silver) was made by Moroz.[11] The first optical studies of reflectivity in MIO were completed on Bi infiltrated opals,[12] followed by Ga MIO.[13] Recently, tungsten inverse opals were experimentally studied.[14] The EM dispersion relations of uniaxial crystals consisting of metallic wires can be studied analytically.[2,15] However the opal geometry is so much more complicated that only numerical computations are possible; these are performed here using a commercial software package.[16]

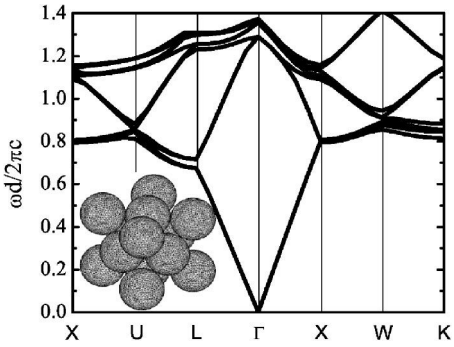

FIG. 1. Photonic band structure of a bare opal. The opal structure is shown in the inset.

The paper is organized as follows. In Sec. II we discuss the computational results of photonic band structures, as well as reflectivity and transmission spectra. Section III describes the sample preparation and experimental results.

II. THEORETICAL STUDIES OF METAL-INFILTRATED OPALS

A. Photonic spectra of MIOs

We start our studies with the simplest case of opal infiltrated by an "ideal" metal. In this approximation the metal in the frequency range of interest is described by a dielectric constant with a large negative real part and small imaginary part. We also assume that the infiltration factor p is close to 1, which means that all empty pores of the opal are completely filled by the metal; consequently, the volume-filling fraction of the metal $f=0.26$. In this case we may neglect the frequency dispersion of the metallic dielectric constant because the EM fields do not penetrate into the metal. The resulting EM dispersion curves are shown in Fig. 2(a). They have a simple quantitative interpretation and may serve as a reference point for interpreting EM band structures in the case of real metal infiltration. An ideal MIO system can be considered as a periodic array of spherical cavities filled by silica and covered by a metal. Since the quality of the metal

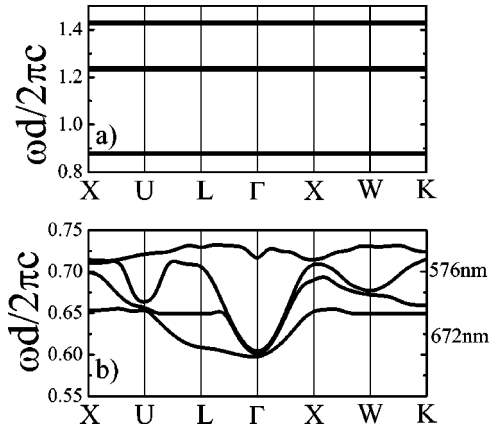

FIG. 2. Photonic band structure of MIO: (a) ideal metal approximation, (b) Ag-infiltrated opal with $p=1$ and $D=285$ nm. Here $d=D\sqrt{2}$, where D is the silica ball diameter.

TABLE I. Comparison of the eigenfrequencies of a spherical resonator surrounded by an ideal metal with the frequencies of the propagating modes in MIO.

Resonator ($\omega d/2\pi c$)	Opal ($\omega d/2\pi c$)
0.88	0.88
1.24	1.23
1.43	1.42

is good, each cavity represents a high-quality resonator. In this case the fields are mostly localized inside the cavities and the interaction between cavities is very weak. Therefore the dispersion of the propagating EM modes is negligible and their frequencies almost coincide with the eigenfrequencies of a single ideal spherical cavity filled with silica. The lowest eigenfrequency of such a cavity is $\omega_c \approx 5.48c/\sqrt{\epsilon_d}D$, where ϵ_d is a dielectric constant of silica.[17] This mode is threefold degenerate since it corresponds to the angular momentum $l=1$. The next mode $\omega \approx 7.78c/\sqrt{\epsilon_d}D$ is fivefold degenerate ($l=2$). In MIO with a real metal this degeneracy is lifted due to interaction with neighboring cavities.

Our computation shown in Fig. 2(a) confirms the validity of such a simple approach (note that $d=D\sqrt{2}$). The comparison between the eigenfrequencies of a single resonator and the EM modes in MIO with an ideal metal is presented in Table I.

Computations of photonic band structures for opals infiltrated with real metals are more complicated because of the frequency dispersion of the dielectric constant, which has been taken from the literature for bulk measurements.[18] The problem is that the standard finite element eigenvalue solvers require specification of material parameters, such as ϵ and μ, as an input. In general, the eigenfrequencies obtained using this procedure do not correspond to the initially chosen material parameters, and thus modification of the standard algorithm is required. A simple iterative procedure that we used here provides solutions with a good convergence and stability. This happens because the dielectric constants of the metals considered here are smooth functions of frequency in the spectral range of interest. In principle, we have a nonlinear eigenvalue problem, where extra solutions are possible and bifurcations might prevent a smooth convergence.

Figure 2(b) demonstrates the photonic band structure of Ag infiltrated opal with $p=1$ and $D=285$ nm. The EM dispersion is larger than in the case of an "ideal" metal, but is still small. The resonator eigenfrequencies are lower for larger diameter silica spheres; metal at such frequencies is closer to being perfect. Therefore the EM dispersion decreases with increasing D (see Fig. 3). The specific properties of opal infiltrated with a good metal is that it has very narrow bands with small group velocity. The fields are mostly concentrated in the silica cavities. Table II summarizes the results obtained for different MIOs.

B. Reflectivity and transmission spectra of MIO

Reflectivity $R(\omega)$ and transmission $T(\omega)$ spectra of thin films of MIO were calculated for silver and lead. We consid-

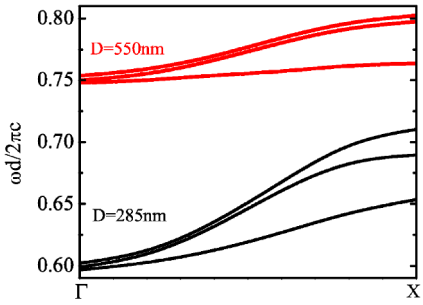

FIG. 3. (Color online) Photonic band structure of Ag MIO with $p=1$, $D=285$ nm (three lowest curves) and $D=550$ nm (three upper curves).

ered a monochromatic plane wave at normal incidence with respect to the MIO crystals, which are cut perpendicular to ⟨100⟩ direction. Figure 4 shows R and T spectra for five-layer silver- and three-layer lead-infiltrated opals, respectively, with $p=1$ and $D=285$ nm. The main feature in $R(\omega)$ is the growth and saturation at long wavelength, which is due to the low-frequency gap in the photonic spectra of MIOs. The first minimum in $R(\omega)$ and maximum in $T(\omega)$ appear because of the existence of propagating EM modes above the cutoff frequency. In fact, the MIO samples that were prepared and studied experimentally (Sec. III) are cut perpendicular to ⟨111⟩ rather than ⟨100⟩ direction. Nevertheless, the frequency region of the propagating EM modes is so narrow that the first minima in reflectivity should be isotropic. The vertical lines in Fig. 4 show positions of ω_Γ and ω_X from the photonic band structures listed in Table II. The low transmission of Pb MIO is explained by a very small group velocity (see $\Delta\omega$ in Table II) and high absorption of the propagating EM modes because of the large imaginary part of Pb dielectric constant.

To compare the computational results with the experimental reflectivity spectra we took into account that the actual opal samples do not have $p=1$ (see details in Sec. III). Therefore the following computational model for the actual MIOs was created. We started with a close-packed fcc lattice of 285 nm silica spheres and increased D while keeping fixed the lattice constant. This procedure was designed to create the sphere overlap, while at the same time the volume fraction of the pores decreases. The diameter was chosen in such a way that the volume fraction of the pores decreased to $\approx 16\%$,

TABLE II. Parameters of the spectra of MIO for various metals and silica ball diameters, where ω_Γ is the cutoff frequency and ω_X is the frequency of the third lowest mode in the X point, $\Delta\omega=\omega_X-\omega_\Gamma$.

Metal and sphere diameter (nm)	$\omega_\Gamma d/2\pi c$	$\omega_X d/2\pi c$	$\Delta\omega/\omega_\Gamma$
Ideal Metal	0.88	0.88	0
W, $D=285$	0.87	0.88	0.01
In, $D=285$	0.65	0.69	0.06
Ag, $D=550$	0.75	0.80	0.07
Pb, $D=285$	0.71	0.76	0.07
Ag, $D=285$	0.6	0.71	0.18

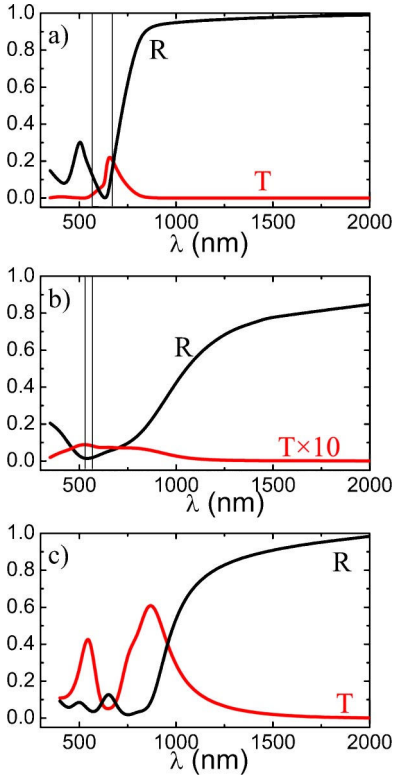

FIG. 4. (Color online) Calculated reflectivity and transmission spectra of (a) five-layer Ag- and (b) three-layer Pb-infiltrated opals with $p=1$, $D=285$ nm, and (c) five-layer Ag-infiltrated opal with the volume fraction of metal 16% (see detailed description in Sec. II B).

whereas the pores were filled by metal (the volume fraction of metal in this system corresponds to an opal with $p=0.6$). Reflectivity and transmission spectra of this model when filled with Ag are shown in Fig. 4(c). Since this MIO has less metal compared to opal with $p=1$, the cutoff frequency is lower and the dispersion of the propagating bands is larger. These qualitative results follow from the model of spherical cavities considered above. Consequently, the first minimum in $R(\omega)$ [Fig. 4(c)] occurs at a larger wavelength compared to that in Fig. 4(a).

III. OPTICAL STUDIES OF METAL-INFILTRATED OPALS

We have fabricated 3D MIOs that consist of infiltrated metals into porous synthetic opal photonic crystals. Two different metals were chosen for the opal infiltration: silver and copper, both having typical metallic properties. The specular reflectivity of the infiltrated and uninfiltrated opals, as well as the pure metals was subsequently measured in a broad spectral range from 0.3 to 25 μm using several combinations of light sources, detectors, and spectrometers. We found that the optical reflectivity spectra of the MIO samples dramatically decrease in the visible/NIR spectral range, recuperating in the mid-IR range below a cutoff frequency. In addition, some of the MIO samples showed relatively bright iridescent colors caused by a broad Bragg stop band in the visible range that was formed because of the enhanced optical penetration

depth in the composites, compared to the skin depth of the pure metals.

A. MIO fabrication

Opal photonic crystals as templates for the metal infiltration were grown by sedimentation of 245, 285, and 550 nm diameter silica balls, respectively in aqueous solutions. The resulting synthetic opals consisted of microcrystals with characteristic size of tens of microns and a preferable vertical orientation along the $\langle 111 \rangle$ crystallographic direction.

Silver and copper were introduced into the bare opal matrix by the chemical bath deposition method.[19] First, the interconnected pore sublattice in the opal samples was impregnated by saturated aqueous solutions of $AgNO_3$ or $Cu(NO_3)_2$. The samples were dried and the salts were reduced by hydrogen. The rate of the hydrogen flow was about 1 sccm (cubic centimeter per minute), and the reduction process temperature was 400°C for both metals. We repeated this procedure periodically to increase the infiltration factor of the opal pores.

The infiltration factor that was controlled by the gravimetric technique was found to be $p=0.6\pm0.05$ for both metals. The results of the gravimetric measurements are reasonable because these metals have much larger densities (Ag, 10.5 g/cm^3; Cu, 8.9 g/cm^3) compared to bare opals (1.3 g/cm^3), and this reduces the uncertainties in determining p.

The resulting MIO samples were approximately $5\times5\times1$ mm^3 with the flat surface area perpendicular to $\langle 111 \rangle$. The surface of the metal-infiltrated opals were mechanically polished prior to the optical-reflectivity measurements. For the polishing we used a diamond powder with grain size of <1 mm. This process does not break any individual silica balls; instead it pulls them off the MIO surface as a whole. We note that the polished surface coincides with the (111) planes in the fcc structure that is, in fact, perpendicular to the direction of the opal growth. This is the reason that it was possible to remove the silica balls from the MIO surface, layer by layer, while creating very few defects. Following the polishing process the MIO samples were checked by scanning electron microscope (SEM), and the best samples were used for the optical measurements.

The obtained MIOs were electrically conductive, showing network topology. We performed additional estimates of the metal-filling factor by several techniques, including measurement of the average density, and also reversing the infiltration by dissolving the metal. We found that the infiltration factor p for Ag and Cu MIOs was 0.6 ± 0.1, in good agreement with p obtained from the gravimetric measurements.

B. Optical measurements

The specular reflectivity $R(\omega)$ from 0.3 to 4.1 μm was measured for the MIOs, metallic films, and uninfiltrated opal samples using a homemade spectrometer. The spectrometer consists of various incandescent light sources (tungsten-halogen and glow-bar lamps), solid-state detectors (enhanced-UV Si, Ge, and InSb), and a 0.3-meter monochromator (Action Research Corporation) that was equipped with several gratings in order to span the required broad spectral range. The measured $R(\omega)$ spectra were also compared to $R(\omega)$ obtained using a Fourier transform infrared spectrometer in the mid-IR spectral range of 2–25 μm by normalizing the spectra at the overlapping spectral range. The incident light beam was directed to be about 13° with respect to the surface normal. The obtained $R(\omega)$ spectra were normalized by that of a gold-plated mirror measured under the same conditions at the respective spectral ranges. The MIO samples were kept at ambient during the measurements.

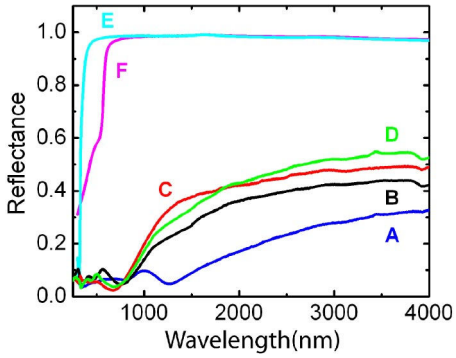

FIG. 5. (Color online) Reflectivity spectra of the fabricated MIOs and metallic films: (a) Ag, $D=550$ nm, $p=0.6$; (b) Ag, $D=285$ nm, $p=0.6$; (c) Cu, $D=245$ nm, $p=0.6$; (d) Ag, $D=245$ nm, $p=0.6$; (e) Ag 200 nm film; and (f) Cu 200 nm film.

A comparison with reflectivity spectra measured using an integrating sphere was also done. The integrating sphere measures the specular as well as the diffused reflectivity. We conclude that for the measured MIO samples using the homemade spectrometer, about half of the light intensity is lost due to diffused reflectivity. Therefore the limiting reflectivity value of 50% at long wavelengths (see Fig. 5) is actually very close to 100% if the diffused reflectivity were collected.

Figure 5 shows the reflectivity spectra of four MIO samples, Ag infiltrated in opals of various silica ball diameters, and Cu infiltrated into opal of 245 nm ball diameter. The $R(\omega)$ of all four samples is small in the visible spectral range, showing that the EM radiation may, indeed, penetrate into the MIOs at these short wavelengths. $R(\omega)$ increases at long wavelengths for all four MIO samples with a threshold at a cutoff wavelength λ_c. λ_c for the three MIO samples with the smaller diameter is about the same at $\approx$700 nm; although λ_c for the smallest silica ball opal is the shortest. For the 550 nm diameter MIO λ_c is about 1300 nm. This agrees well with the ratio between the silica ball diameters of the various MIO samples. We get $\lambda_{c,b}/\lambda_{c,s}\approx D_b/D_s\approx 1.9$, where $\lambda_{c,b}(\lambda_{c,s})$ is λ_c for the MIO with the big D_b (small D_s) silica ball diameter; this is in good agreement with the simple model presented in the introduction. In conclusion, $R(\omega)$ general appearance and cutoff wavelengths are in very good agreement with the calculated spectra presented in Fig. 4(c).

IV. SUMMARY

In summary, we have shown that the optical properties of synthetic opal photonic crystals infiltrated with metals can be

qualitatively understood using a simple model of weakly interacting spherical resonators. Photonic band structures for opals infiltrated with Ag, W, In, and Pb have been calculated where the dielectric constant dispersion of the metal was taken into account. The propagating EM bands are narrow, and for a good metal they are separated by the omnidirectional band gaps. Reflectivity and transmission spectra for thin-film MIO were calculated for Ag- and Pb-infiltrated opals. Opal samples were fabricated and infiltrated by Ag and Cu using the chemical-bath deposition method. Reflectivity spectra were measured in the visible and mid-IR spectral range and were found to be in a good agreement with the computational results.

ACKNOWLEDGMENTS

This work was funded by the NSF, Grant No. DMR-0102964. A.E. and C.Y.L. were partially supported by the Seed Grant of the University of Utah. Z.V.V. and V.K. were partially supported by ARO Grant No. DAAD 19-03-1-0290. Discussions with J. Shi and S. Blair are greatly appreciated.

*Electronic address: efros@physics.utah.edu

[1] J. B. Pendry, A. J. Holden, W. J. Stewart, and I. Youngs, Phys. Rev. Lett. **76**, 4773 (1996).
[2] A. L. Pokrovsky and A. L. Efros, Phys. Rev. Lett. **89**, 093901 (2002).
[3] A. A. Zakhidov, R. H. Baughman, Z. Iqbal, C. Cui, I. Khayrullin, S. O. Dantas, J. Marti, and V. G. Ralchenk, Science **282**, 897 (1998).
[4] B. T. Holland, C. F. Blanford, and A. Stein, Science **281**, 538 (1998).
[5] J. Zhou, Y. Zhou, S. L. Ng, H. X. Zhang, W. X. Que, Y. L. Lam, Y. C. Chan, and C. H. Kam, Appl. Phys. Lett. **76**, 3337 (2000).
[6] O. D. Velev, P. M. Tessier, A. M. Lenhoff, and E. W. Kaler, Nature (London) **401**, 548 (1999).
[7] J. E. G. J. Wijnhoven, S. J. M. Zevenhuizen, M. A. Hendriks, D. Vanmaekelbergh, J. J. Kelly, and W. L. Vos, Adv. Mater. (Weinheim, Ger.) **12**, 888 (2000).
[8] V. G. Golubev, J. L. Hutchison, V. A. Kosobukin, D. A. Kurdyukov, A. V. Medvedev, A. B. Pevtsov, J. Sloan, and L. M. Sorokin, J. Non-Cryst. Solids **299**, 1062 (2002).
[9] C. Lopez, Adv. Mater. (Weinheim, Ger.) **15**, 1679 (2003).
[10] B. T. Mayers, B. Gates, and Y. Xia, Adv. Mater. (Weinheim, Ger.) **12**, 1629 (2000).
[11] A. Moroz, Phys. Rev. Lett. **83**, 5274 (1999).
[12] N. Eradat, J. D. Huang, Z. V. Vardeny, A. A. Zakhidov, I. Khairullin, I. Udod, and R. H. Baughman, Synth. Met. **116**, 501 (2001).
[13] V. Kamaev, V. Kozhevnikov, Z. V. Vardeny, P. B. Landon, and A. A. Zakhidov, J. Appl. Phys. **95**, 2947 (2004).
[14] G. Freymann, S. John, M. Schultz-Dobrick, E. Vekris, N. Tetreault, S. Wong, V. Kitaev, and G. A. Ozin, Appl. Phys. Lett. **84**, 224 (2004).
[15] A. L. Pokrovsky and A. L. Efros, Phys. Rev. B **65**, 045110 (2002).
[16] FEMLAB, *Reference Manual, Version 2.2* (Comsol AB, Sweden, 1994).
[17] L. D. Landau and E. M. Lifshitz, *Electrodynamics of Continuous Media* (Pergamon Press, Oxford, 1960).
[18] M. A. Ordal, L. L. Long, R. J. Bell, S. E. Bell, R. R. Bell, R. W. Alexander, and C. A. Ward, Appl. Opt. **22**, 1099 (1983).
[19] V. G. Golubev, V. Yu. Davydov, N. F. Kartenko, D. A. Kurdyukov, A. V. Medvedev, A. B. Pevtsov, A. V. Scherbakov, and E. B. Shadrin, Appl. Phys. Lett. **79**, 2127 (2001).